JOURNAL OF GEOPHYSICAL RESEARCH, VOL. 87, NO. A1, PAGES 111-117, JANUARY 1, 1982

Magnetic Field Line Reconnection Experiments 4. Resistivity, Heating, and Energy Flow

R. L. STENZEL, W. GEKELMAN, AND N. WILD

Department of Physics, University of California, Los Angeles, California 90024

Detailed spatial and temporal measurements of the total vector electric field **E** and current density **J** in a plasma with dynamic magnetic field line reconnection have been made. The resistivity calculated via the generalized Ohm's law is found to be spatially inhomogeneous with values exceeding the classical resistivity by 1 to 2 orders of magnitude. Resistivity and current density do not maximize in the same locations. The dissipation $\mathbf{E} \cdot \mathbf{J}$ is determined and analyzed in terms of particle heating and fluid acceleration. Electron heating is found to be the dominant dissipation process in the diffusion region. Independent measurements of the divergence of the Poynting vector $\nabla \cdot (\mathbf{E} \times \mathbf{H})$, the change in stored magnetic field energy $\partial/\partial t(B^2/2\mu_0)$, and the dissipation give a consistent, detailed picture of the energy flow. Efficient conversion of electromagnetic energy into particle heating is observed.

INTRODUCTION

The interest in magnetic field line reconnection arose in the early studies of solar flares [*Giovanelli,* 1948] and has subsequently expanded to other phenomena such as magnetic substorms [*McPherron,* 1979] and comets [*Niedner and Brandt,* 1978]. The basic common problem in these areas is to find an explanation for the observed strong transfer of magnetic field energy to particle kinetic energy. Currents usually flowing in regions of magnetic null points are thought to give rise to various microinstabilities. These increase the effective resistivity, leading to enhanced particle heating and diffusion of field lines. Tearing instabilities cause dynamic changes in the magnetic fields, which give rise to large inductive electric fields and strong particle accelerations [*Pellinen and Heikkila,* 1978; *Coroniti et al.,* 1977]. However, it is generally acknowledged that the plasma dynamics in neutral points is rather complex and that because of observational difficulties a clear picture of reconnection processes has not yet emerged [*Frank and Ackerson,* 1979]. Recently, numerical simulations have been extensively employed to aid the understanding of the problems [*Birn,* 1980; *Leboeuf et al.,* 1981].

We have started to investigate magnetic field line reconnection in a large laboratory plasma [*Stenzel and Gekelman,* 1979]. Even though the actual parameters of a space plasma configuration cannot be scaled exactly, the essential features of the reconnection process can be established and then investigated in far greater detail than is possible in nature. Such approaches have been undertaken earlier [*Bratenahl and Yeates,* 1970; *Ohyabu and Kawashima,* 1972; *Syrovatskii et al.,* 1973], but only in small collision dominated plasmas with incomplete diagnostics. The present experiment is performed in a large, nearly collisionless plasma which is rapidly pulsed and highly reproducible from shot to shot. It is diagnosed internally with various probes, and with the aid of an on-line digital computer a large amount of information is acquired, processed, and displayed in a condensed form as time-space diagrams. Different aspects of the work have been described in a sequence of papers of which this is the fourth part. The first two papers, referred to as part 1 [*Stenzel and Gekelman,* 1981] and part 2 [*Gekelman and Stenzel,* 1981] describe magnetic field topologies and plasma properties, respectively. Part 3 [*Gekelman et al.,* 1981], the companion paper to the present part 4, deals with the plasma dynamics. Here we describe the important subjects of plasma resistivity and energy transfer.

Direct measurements of the plasma resistivity are quite difficult to perform, particularly in a dynamic neutral sheet experiment. During the early phase of research, investigators have derived the resistivity from the ratio of the axial inductive electric field component and axial current density [*Baum et al.,* 1973]. Frank [1976] obtained the plasma resistance by simply dividing the total axial voltage by the plasma current. These interpretations of plasma resistances yielded anomalously large values inconsistent with the observed low heating. Recently, it has been observed that polarization, or space charge, electric fields comparable to the inductive electric fields exist [*Stenzel and Gekelman,* 1979; *Baum and Bratenahl,* 1980b]. Space charge and inductive electric fields are in opposite directions over most of the plasma volume, resulting in a small net electric field, except at the cathode sheath. Aside from the electric field, pressure gradients and Hall fields also contribute to the current flow. Furthermore, currents and fields also have vector components perpendicular to the neutral sheet. Thus a careful analysis of the plasma resistivity requires in situ measurements of all electric field and current density vectors as well as plasma pressures, flows, and magnetic fields. This has been done in our experiment, which enables us to calculate the resistivity from the generalized Ohm's law. It is found that the resistivity is spatially very inhomogeneous but does not simply maximize in regions of large current densities, as is often assumed in computer simulations [*Ugai and Tsuda,* 1977; *Hayashi and Sato,* 1978]. On the average the resistivity can exceed the classical value by 1 order of magnitude, at local maxima by even 2 orders.

From the knowledge of currents and electric fields (or resistivities) the dissipation of electromagnetic energy $P = \mathbf{E} \cdot \mathbf{J} = \eta J^2$ can be readily determined. The dissipation leads to an increase in particle kinetic energies, partly by enhancing the random motion (heating) and partly the directed motion (acceleration). The energy input into the plasma does not lead to an unlimited temperature or velocity rise but is soon balanced by energy losses. For example, inelastic atomic collisions transfer kinetic electron energy into multiple

Paper number 1A1407.
0148-0227/82/001A-1407$01.00

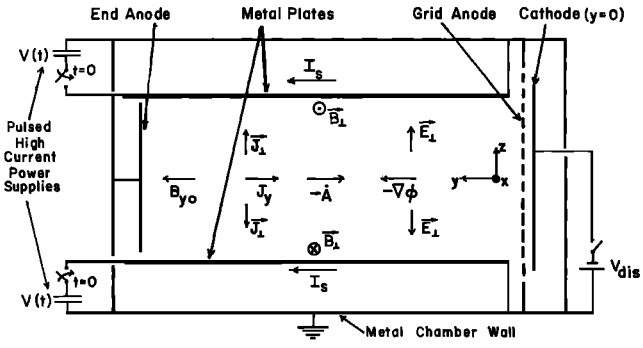

Fig. 1. Schematic diagram of currents, electric fields, and magnetic fields in a side view of the experimental arrangement.

ionization and line radiation. From the observed increase in the random energy density of the plasma ΔnkT and the directed energy density $\frac{1}{2}nmv_d^2$, we conclude the dissipation leads largely to electron heating and less to the formation of accelerated ions. This result is in contrast to predictions from earlier experiments [*Ohyabu et al.*, 1974*b*] and computer simulations [*Sato et al.*, 1978] but is interesting to compare with observations of 'fireballs' in the magnetotail [*Frank et al.*, 1976].

Lastly, we can account for the energy flow in this experiment. For a test volume of plasma around the neutral sheet we have calculated both inflow and outflow of the Poynting vector, i.e., $-\nabla \cdot (\mathbf{E} \times \mathbf{H})$, and show that it is the time rate of change of stored field energy $\partial/\partial t(B^2/2\mu_0)$ and the internal dissipation $\mathbf{E} \cdot \mathbf{J}$. These results do not only show the consistency of the independent measurements but also indicate that a large fraction (~80%) of the electromagnetic energy is dissipated, while the small remainder builds up magnetic field energy. The large dissipation cannot be explained on the basis of the classical plasma resistivity but results from an anomalous resistivity.

The experimental observations grouped in various topics will be described and discussed in the next section. The final section summarizes the significant findings and points out further investigations.

Experimental Results

We will first present data on the basic parameters such as electric fields and currents. These are measured under identical conditions as magnetic fields and other plasma parameters described earlier. All the data will then be combined to yield the resistivity, dissipation, and energy flow.

Electric Fields

In order to discuss the electric field measurements it is useful to start with a schematic diagram of the experiment, shown in Figure 1. It indicates the important physical parameters in a side view of the device; a cross-sectional view was given in Figure 1 of part 3.

The time-varying current I_s pulsed through the metal plates generates the time-varying transverse magnetic field $\mathbf{B}_\perp$, which in turn gives rise to an axial-induced (rotational, $\nabla \times \mathbf{E}_i = -\dot{\mathbf{B}}_\perp$) electric field $E_i = -(\partial A/\partial t) = -\dot{A}$, where $\mathbf{A}$ is the vector potential ($\nabla \times \mathbf{A} = \mathbf{B}$). This field is the primary mechanism for driving axial plasma currents J_y. The induced electric field is measured as shown schematically in Figure 2*a*. A loop probe is inserted into the plasma. It consists of two radial wires connected by a short axial section of length Δy which can be placed along the separator (neutral line). The open-loop voltage V arises only from the induced voltage on the axial section, so that $-\dot{A}_y = V/\Delta y$ is readily determined.

If, instead, the two insulated radial wires are terminated by Langmuir probes, the local plasma potential $\phi_p(y)$ and $\phi_p(y + \Delta y)$ can be measured. As discussed in part 2 (Figure 8) such measurements reveal the presence of a strong axial potential gradient, hence an irrotational electrostatic field $E_s = -\nabla\phi_p$ builds up in response to the applied induced electric field and pressure gradients. The two field contributions are in opposite directions and of comparable magnitude such that the net electric field $E_y = -\dot{A}_y - \nabla_y\phi_p$ is much smaller than $-\dot{A}_y$. Locally, E_y can be antiparallel to $-\dot{A}_y$, but averaged over the x-z plane, E_y and $-\dot{A}_y$ are in parallel.

The net electric field can, in principle, be obtained from the two separate measurements of $\dot{A}$ and $\nabla\phi_p$ but the accuracy is greatly improved if the subtraction of two comparable quantities is performed instantaneously and in situ with a differential probe, shown in Figure 2*b*. It consists of two insulated radial probe shafts with short axial sections of length Δy terminated by two identical Langmuir probes. Both probes are swept with the same fast ramp voltage $V_{(t)}$ and their currents I_1, I_2 are recorded simultaneously with 20 MHz, eight-bit analog-digital converters. The knees in the two probe characteristics are associated with sweep voltages V_1 and V_2, respectively, which differ not only by the local plasma potentials but also by the induced voltages $\pm\dot{A}\Delta y$ on the axial wire sections. The voltage difference per axial length yields the net electric field $\Delta V/2\Delta y \simeq -\nabla_y\phi_p - \dot{A}_y$. The differential probe is movable in the x-z plane and swept at seven different times during the reconnection event so as to obtain the space-time behavior of the net axial electric field shown in Figure 3*a*.

With a single, radially inserted Langmuir probe the elec-

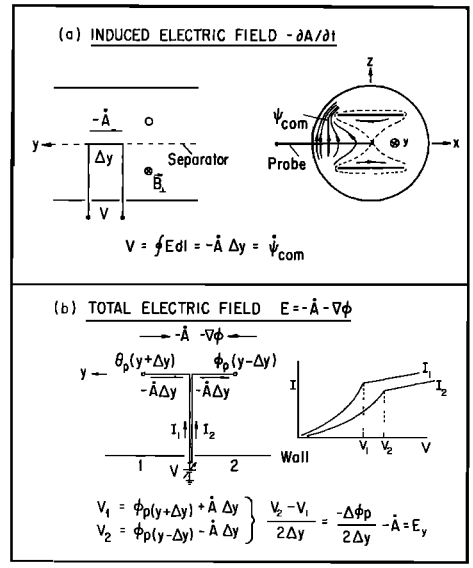

Fig. 2. Measurement principle for determining electric fields. (a) Loop probe for measuring the induced axial electric field $-\dot{A}_y$. (b) Differential Langmuir probe for determining the sum of induced (rotational) and space charge (irrotational) electric fields $E_y = -\dot{A}_y - \nabla_y\phi_p$.

tron density and temperature are recorded as described in part 2. From these results it is shown in part 3 (Figures 3 and 7) that the plasma pressure exhibits large gradients in the transverse x-z plane. An equivalent electrostatic field $\mathbf{E}_\perp = (1/ne)\,\nabla_\perp nkT_e$ has been calculated (part 3, Figure 7*b*). It is approximately consistent with the transverse gradients in the plasma potential observed directly (part 2, Figure 7). Thus even though we did not apply any induced electric fields in the perpendicular direction ($A_\perp \simeq 0$), and the plate potential cannot penetrate beyond a few Debye lengths ($\lambda_D \simeq 0.02$ mm), the plasma self-consistently develops an internal space charge electric field of magnitude larger than the net axial field ($E_\perp > E_y$). The spatial distribution of $\mathbf{E}_\perp$ is shown in Figure 3*b*.

Due to the motion of the fluid the particles in the moving frame experience another electric field component, the Hall field $\mathbf{v} \times \mathbf{B}$. Having measured all components of the fluid velocity $\mathbf{v}$ (part 3, Figures 9 and 11) and of the magnetic field (part 1, Figures 6–11) we have calculated $\mathbf{v} \times \mathbf{B}$ in direction and magnitude. In the axial direction the Hall field contributes only near the edges of the neutral sheet where the outflow velocities are large [$(v_\perp \times B_\perp)_{max} < 0.1$ V/cm]. In the transverse plane the Hall field contributions are more than an order of magnitude below the electrostatic fields. Hence for practical purposes we can neglect the Hall current contribution in our experiment.

At the present stage of the experiment we consider only the average electric fields and not the fluctuations which are lost by forming ensemble averages over typically 10 shots per data point. Fluctuating fields caused by microinstabilities, however, do play an important role and will be investigated separately.

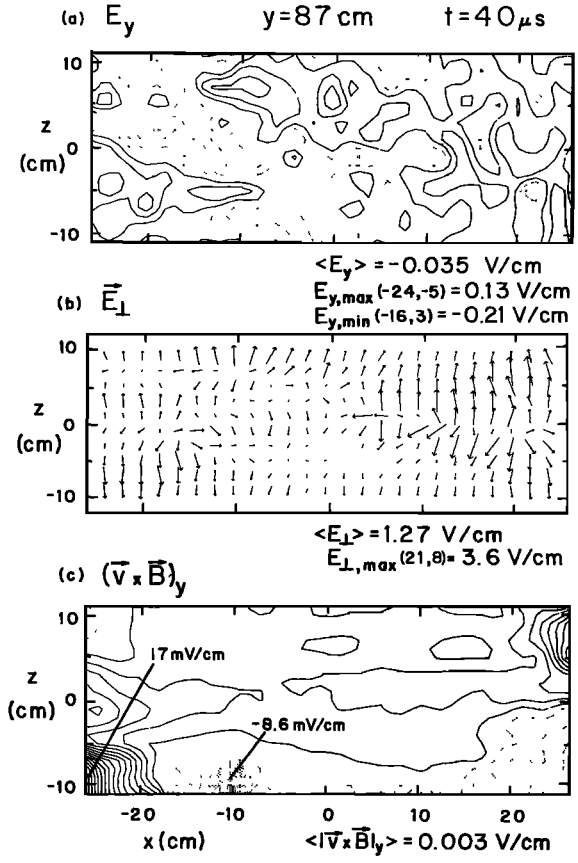

Fig. 3. Electric field components in the x-z plane at $y = 87$ cm from the cathode and $t = 40$ μs. (a) Contours of constant net axial electric field E_y. Contour spacing 0.05 V/cm. (b) Vector field of the transverse electric field caused by pressure gradients $\mathbf{E}_\perp = 1/ne\ \nabla_\perp (nkT_e)$. (c) Contours of constant Hall electric field in axial direction $E_{Hy} = (\mathbf{v} \times \mathbf{B})_y$. Contour spacing 1 mV/cm.

Currents

In response to the applied and self-consistently developing electric fields, plasma currents are flowing. The dominant neutral sheet current ($I_p > 1000$ A) flows axially and is carried by electrons drifting from the cathode toward the end anode. Space charge neutrality is approximately preserved since electrons collected at the end anode are replaced by electrons emitted from the cathode. However, the cathode emission is space charge limited, i.e., the emitted electron current is linked to the collected ion current by the Langmuir criterion $I_e/I_i \simeq (m_i/m_e)^{1/2}$ [*Langmuir*, 1929]. Thus by applying an induced electric field on the order of the runaway field [*Dreicer*, 1959] a collisionless plasma responds by setting up a space charge field, which partly offsets the applied field and limits the electron drift to $v_d < v_e$.

The axial current density $J_y(x, z)$ is measured either directly with a differential Langmuir probe, as described in part 2 (Figure 1*b*), or indirectly from the magnetic field data by evaluating $J_y = (\nabla \times \mathbf{H})_y$, as shown in Figure 12*a* of part 1. Similarly the transverse current density $\mathbf{J}_\perp = (J_x, J_z)$ is found from magnetic field measurements $\mathbf{J}_\perp = (\nabla \times \mathbf{H})_\perp$, an example of which is shown in Figure 12*b* of part 1. The perpendicular currents arise partly from $\mathbf{E} \times \mathbf{B}$ drifts associated with the transverse space charge fields (Figure 3*b*), and partly they represent projections of the field-aligned currents into the x-z plane. It should be recalled that the resultant magnetic field lines are increasingly sheared with transverse distance from the neutral sheet. Currents are not only confined to the neutral sheet regions but can also flow on sheared flux tubes connecting cathode and end anode, although subject to mirror effects caused by field strength variations along these lines of force. The transverse current densities are, on the average, 1 order of magnitude smaller than the axial ones.

Resistivity

Measurements of the electron density and temperature (part 2) lead to the conclusion that for $t \gtrsim 25$ μs the plasma becomes essentially fully ionized, since the density remained constant while the electron temperature kept rising ($kT_{e\,max} \simeq U_i$, ionization energy). Thus a two-fluid model seems appropriate for analyzing the plasma resistivity defined by the generalized Ohm's law [*Delcroix*, 1965]. Neglecting the inertial currents ($\partial/\partial t \ll \nu_e$) it is given by

$$\eta \mathbf{J} + \frac{1}{ne}\,\mathbf{J} \times \mathbf{B} = \mathbf{E} + \mathbf{v} \times \mathbf{B} + \frac{1}{ne}\,\nabla(nkT_e) \qquad (1)$$

where we assumed a scalar resistivity η.

Having measured all contributions on the right-hand side that give rise to current flows (denoted by $\mathbf{E}_{tot}$) as well as the current density vector $\mathbf{J}$, we have calculated the resistivity $\eta = \mathbf{E}_{tot} \cdot \mathbf{J}/\mathbf{J}^2$ and normalized it to the classical Spitzer resistivity η_s [*Spitzer*, 1962]. The enhancement factor η/η_s is determined at every position (x, z) and at different times during the reconnection event. A typical result ($t = 40$ μs) is

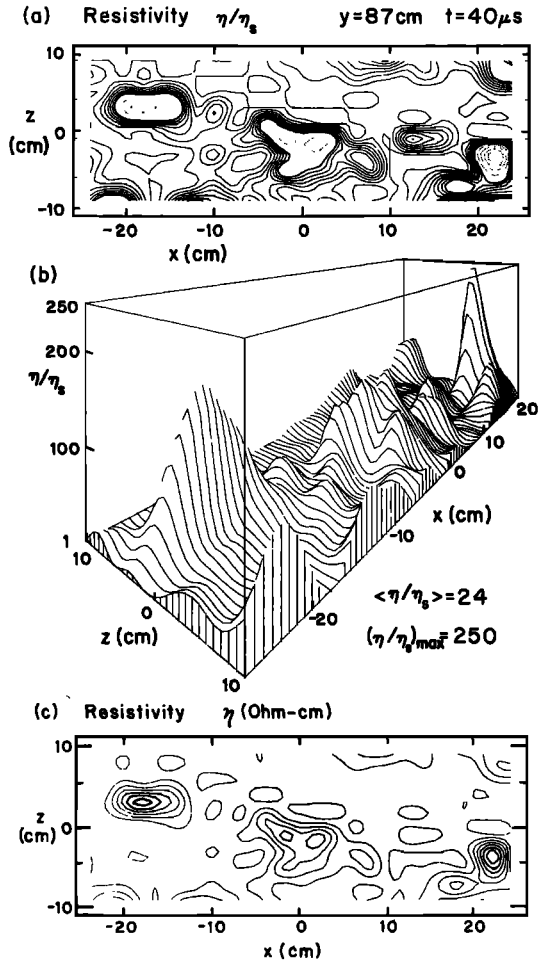

Fig. 4. Measured resistivity, both absolute and normalized to the local Spitzer resistivity, at $t = 40$ μs. (a) Contours of constant normalized resistivity $\eta_{(x,z)}/\eta_{s(x,z)}$. Contour spacing 20 (solid lines), 40 (dotted lines). (b) Three-dimensional view of the normalized resistivity. (c) Contours of constant absolute resistivity $\eta_{(x,z)}$, $\eta_{max} = 1.67$ Ωcm at $(x, z) = (-16, 2)$ cm, spatial average $\langle\eta\rangle = 0.22$ Ωcm, contour spacing $\Delta\eta = 0.25$ Ωcm.

shown in Figure 4, which indicates the spatial nonuniformity of the plasma resistivity. The resistivity does not simply maximize in the curent sheet but exhibits large values near the edges of the neutral sheet where the electron temperature peaks (part 2, Figure 5c). Averaged over the x-z plane the resistivity is 24 times larger than the classical value, and at the local maxima the enhancement is about 2 orders of magnitude. From these observations we can only conclude that a very complex turbulence pattern exists in the neutral sheet region, which is in contrast to many theoretical models. An analysis of the microinstabilities in the neutral sheet has been started, and results will be presented in a later publication.

Dissipation

While the ratio of electric fields and currents yields the resistivity, the product represents the dissipation of electromagnetic energy in the plasma $P = \mathbf{E} \cdot \mathbf{J} = \eta J^2$. We have calculated its space-time variation since it is a crucial parameter in the energy balance and plasma heating.

Figure 5 shows contour plots of the dissipation $P_{(x,z)}$ at $t = 40$ μs. The total power density is broken up into $P = P_\perp + P_y$, where $P_\perp = \mathbf{E}_\perp \cdot \mathbf{J}_\perp$ is the dissipation associated with transverse fields and currents, and $P_y = E_y \cdot J_y$ is the axial dissipation. While the axial currents are considerably larger than the transverse ones, the reverse holds true for the electric fields. Thus the power densities are comparable ($\langle P_\perp\rangle \simeq \langle P_y\rangle$), indicating how important it is to consider all three vector components of E and J. The total dissipation maximizes near the edges of the neutral sheet (see part 1, Figure 7a) in approximately the same regions [$(x, z) \simeq (15, 3)$ cm and $(-20, 2)$] where the energy density nkT_e shows large increases (see part 3, Figure 4a). Knowing the power density ($P_0 = 50$ mW/cm^3) required to preionize the gas to an initial energy density of $(nkT_e)_0 \simeq 10^{-6}$ J/cm^3 one may expect that together with the added dissipation in the reconnection event ($\Delta P \simeq 215$ mW/cm^3) the energy density should increase by a factor 265/50 = 5.3, which is roughly consistent with the observed increase by a factor ~6 near the dissipation maximum. Thus both qualitatively and quantitatively the independent measurements of dissipation and plasma pressure are in reasonable agreement.

Since dissipation and resistivity have been determined from measurements of several physical parameters, it is necessary to discuss the accuracy of the final result. Magnetic field measurements are considerably more accurate than electric field measurements. In particular, the small, net axial electric field E_y that results from the difference between electrostatic and inductive field contributions is difficult to

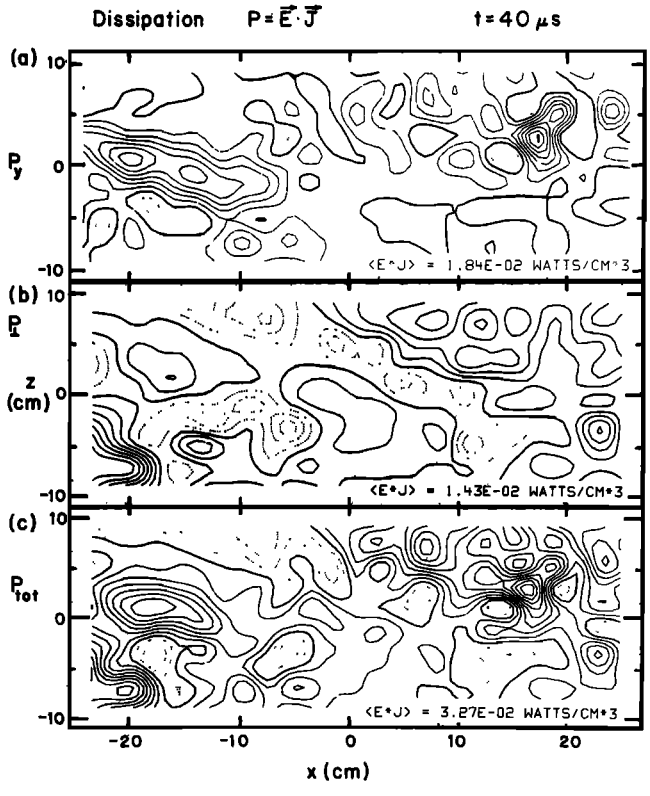

Fig. 5. Contours of constant dissipation $P = \mathbf{E} \cdot \mathbf{J}$ at $t = 40$ μs, showing the spatial distribution $P_{(x,z)}$. (a) Dissipation caused by axial fields and currents $E_y \cdot J_y$. (b) Dissipation by transverse components $\mathbf{E}_\perp \cdot \mathbf{J}_\perp$. (c) Total dissipation $P = E_y \cdot J_y + \mathbf{E}_\perp \cdot {}_\perp\mathbf{J}$. Contour spacing 25 mW/cm^3. Solid contours $\mathbf{E} \cdot \mathbf{J} > 0$, dotted contours $\mathbf{E} \cdot \mathbf{J} < 0$. Regions of negative total dissipation are due to cumulative measurement errors; $\langle P_-/P_+\rangle \simeq 20\%$.

determine with errors less than ~20%. While individual components of the dissipation $\mathbf{E} \cdot \mathbf{J} = E_x J_x + E_y J_y + E_z J_z$ can have a negative sign (see Figure 5*a*, *b*, dotted contours), their sum must be positive in a dissipative medium ($\mathbf{E} \cdot \mathbf{J} > 0$). Our measurements indicate, however, that in a few regions $\mathbf{E} \cdot \mathbf{J} < 0$ (Figure 5*c*, dotted contours), which we do not interpret as a generator action ($|\mathbf{v} \times \mathbf{B}| \ll |\mathbf{E}|$) but by the result of cumulative measurement errors. When integrated over the *x*-*z* plane the ratio of negative to positive dissipation values amounts to $\langle P_-/P_+ \rangle \simeq 20\%$, which can be considered as an estimate for the average measurement error. A similar value applies for the resistivity data (Figure 4). However, in order to avoid confusion associated with negative resistivities we have chosen to display all negative values by the local Spitzer resistivities.

The temporal variation of the dissipation is indicated in Figure 6, which displays $P_{(x,z)}$ at different times $t = 25, 40, 80$ μs. Both near the turn-on of the external current pulse ($t = 0$) and the current maximum ($t \simeq 80$ μs) the dissipation is small, since either currents or electric fields vanish. The dissipation peaks at an intermediate time of $t \simeq 40$ μs. Similar to the resistivity the dissipation is more than an order of magnitude larger than expected on the basis of Coulomb collisions.

Energy Flow

Since the energization of plasma is the central point in the reconnection problem it is important to trace the energy flow

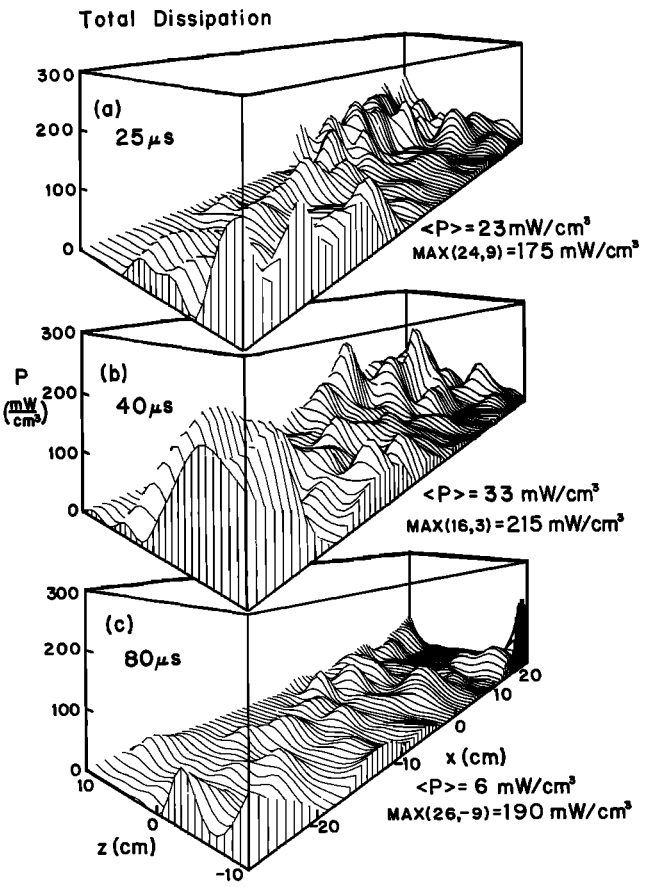

Fig. 6. Three-dimensional views of the total dissipation $P_{(x,z)}$ at different times, 25, 40, and 80 μs, showing the temporal variation. Average value $\langle P \rangle$, maxima $P_{\max(x,z)}$, and minima (classical) $P_{\min(x,z)}$ are indicated.

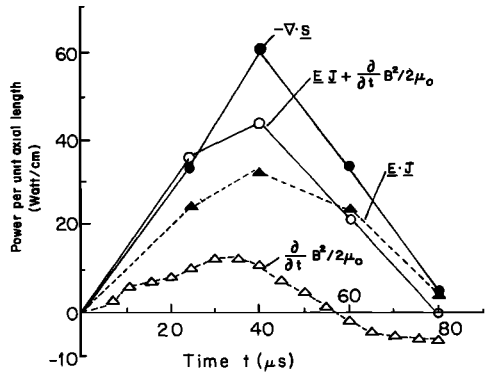

Fig. 7. Temporal variation of the different power terms in the energy flow equation (2). Note that all power densities are integrated over the *x*-*z* cross section and expressed as power per unit axial length. The independently measured terms confirm the conservation of energy flow and show the high conversion rate from electromagnetic to kinetic energy.

from fields to particles. Various attempts have been made in earlier reconnection experiments to account for the energy flow [*Ohyabu et al.*, 1974*a*; *Baum and Bratenahl*, 1980*a*]. Typically, a macroscopic approach is taken where the electrical input power and the outflow of energetic particles are measured and compared. This analysis has many limitations since it is device dependent, ignores boundary phenomena, and tells little about the internal energy conversion processes. Our approach is to leave out the boundary effects and to consider an internal volume of plasma in which we account for the various forms of energy.

According to the Poynting theorem

$$-\nabla \cdot (\mathbf{E} \times \mathbf{H}) = \mathbf{E} \cdot \mathbf{J} + \frac{\partial}{\partial t}\left(\frac{1}{2}\varepsilon_0 E^2 + \frac{1}{2} B^2/\mu_0\right) \quad (2)$$

the divergence of electromagnetic energy flow is given by dissipation and buildup of stored field energy. Having measured the space-time variation of fields and currents we choose a rectangular volume $\Delta V = \Delta x\, \Delta z\, \Delta y = 20 \times 50 \times 1$ cm^3 centered at $x = z = 0$, $y = 87$ cm, and calculate the difference of inflow and outflow of the Poyntings vector $\mathbf{E} \times \mathbf{H}$ through all surfaces. Separately, the dissipation $\mathbf{E} \cdot \mathbf{J}$ and the stored field energy density $B^2/2\mu_0 \gg \varepsilon_0 E^2/2$ are integrated over the volume, and the time derivative $\partial/\partial t(B^2/2\mu_0)$ is formed.

Figure 7 shows the various parts of the conservation equation (2) at different times during the rise of the external current. Since integrated over the *x*-*z* cross section and an axial length $\Delta y = 1$ cm we plot, instead of power densities, the average power per unit axial length in Watts per centimeter. Since both $\mathbf{E}_{(t)}$ and $\mathbf{H}_{(t)}$ vary approximately sinusoidally in time with ~90° phase shift, the electromagnetic power input $-\nabla \cdot (\mathbf{E} \times \mathbf{H})$ also varies sinusoidally, but at half the period $T/2 \simeq 80$ μs. The latter is closely matched by the sum of powers dissipated and required to build up field energy, $\mathbf{E} \cdot \mathbf{J} + \partial/\partial t(B^2/2\mu_0)$, which indicates that the independent measurements are consistent with the required continuity of the energy flow, equation (2). The time rate of change of the energy density varies approximately as $\partial/\partial t(B^2/2\mu_0) \propto \sin 2\omega t$ since $B_{(t)} \propto \sin \omega t$, but noticeable deviations from this dependence arise because of the plasma currents of nonsinu-

soidal dependence (see part 1, Figure 14*a*). Most interesting, however, is a comparison between $\mathbf{E} \cdot \mathbf{J}$ and $\partial/\partial t(B^2/2\mu_0)$, which shows that more than 80% of the total electromagnetic power is dissipated, and less than 20% changes the stored field energy.

The dissipation of electromagnetic energy increases the kinetic energy density of the particles, and it is interesting to examine its partitioning into particle heating, bulk acceleration, and formation of fast runaway electrons or ions. First, we have calculated the energy density associated with the fluid acceleration $\frac{1}{2}\, nm_i v^2$ and compared it with the thermal energy density nkT_e. Except near the edges of the plane where the drift velocity approaches the sound speed, one finds $\frac{1}{2}\, nm_i v^2 \ll nkT_e$, and when averaged over the transverse cross sectoin $\langle \frac{1}{2}\, nm_i v^2 \rangle \simeq 0.05\, \langle nkT_e \rangle$. We conclude that bulk acceleration is less important in the energy flow than electron heating. The ion temperature is, in general, smaller than the electron temperature, but accurate values have not yet been obtained, since the resolution of retarding grid velocity analyzers is limited at these high densities by space charge effects between the grids ($kT_i \lesssim 3$ eV). From the probe characteristics (part 2, Figure 1) no strong evidence is found for runaway electrons or ions. However, observations of enhanced microwave emission near the plasma frequency ($\omega/2\pi \simeq 10$ GHz) indicate the possible generation of some beamlike electrons, but their importance in the overall energy balance is believed to be small.

In spite of the large, continued energy transfer to the electrons, their temperature rise is limited to peak values $(kT_e)_{\max} \simeq 14$ eV and spatial averages $\langle kT_e \rangle \simeq 8$ eV. This saturation is to be expected because of energy sinks for the electrons, such as inelastic collisions (ionization, excitation, $\gtrsim$15 eV/collision) and heat transport along the separator to the end anode. A detailed heat flow analysis, however, is beyond the scope of the present investigation, since the transport coefficients cannot be assumed to be classical.

CONCLUSIONS

The present reconnection experiment has produced a variety of new observations which will now be summarized and compared with earlier work. We have studied the self-consistent interaction of a time-varying magnetic field with a compressible plasma. This approach differs from a class of reconnection experiments [*Ohyabu and Kawashima,* 1972; *Syrovatskii et al.,* 1973; *Overskei and Politzer,* 1976] in which a separate energy source is used to drive currents through a plasma imbedded in a quasi-stationary quadrupole magnetic field. Those arrangements resemble turbulent heating experiments [*Alexeff et al.,* 1969; *Hamberger and Jancarik,* 1972], except for the neutral point magnetic field topology. Our experiment also differs from the class of hyperbolic and *Z* pinch experiments [*Bratenahl and Yeates,* 1970; *Zukakishvili et al.,* 1978] in which plasma production and time-varying magnetic fields are coupled, and the entire current associated with the magnetic field production has to return through the plasma. Current disruptions are characteristic for both classes of experiments where a large current supplied from an external supply is forced through the pulsed plasma. However, these disruptions are localized, typically occurring at the neutral line, and cause only minor variations in the total current [*Baum and Bratenahl,* 1980*a*; *Ohyabu et al.,* 1974*a*], hence should be considered as shifts in the current distribution rather than major disruptions as occur in tokamaks [*Mirnov and Semenov,* 1977]. The associated inductive voltage spikes and local current drops have, up to 1980, been explained by the onset of anomalous resistivity caused by current-driven microinstabilities, but this interpretation is not convincing since it is based on incorrect resistivity measurements. Recently, *Beeler* [1979] repeated electric field measurements in a double inverse pinch and found, during impulsive flux transfer events, a space charge electric field opposing the inductive electric field and, hence, no sudden onset of anomalous resistivity. *Baum and Bratenahl* [1980*b*] now postulate the existence of a double layer at the end of their device. In our experiment we find anomalous resistivity throughout the period of strong current flow. There are fluctuations but no disruptions of the induced current along the neutral line. The latter may be caused by the loss of plasma near the separator, which does not occur in our large discharge plasma. The physics of current disruptions is still poorly understood.

A general difference between reconnection events set up in the laboratory and in space plasmas lies in the cause-effect relation between fields and fluid motions. In most, but not all, laboratory experiments a time-varying magnetic field is applied, causing the plasma to move toward an X-type neutral point. In models describing the events in space [*Vasyliunas,* 1975] a plasma flow causes magnetic field lines to be carried into the diffusion region where both motions become uncoupled and reconnection takes place. Subsequently, the reconnected field lines exit through the convection region where fluid and field line motions are perfectly coupled, leaving at the Alfvén speed. In these steady state theories, whose applicability to actual observations in space has often been questioned, an important problem is the reconnection rate. It is proportional to the energy conversion rate and can be expressed by the normalized inflow velocity of plasma at distances far from the null point $M = v/v_A$. However, this definition applies only to steady state models, and different model-dependent definitions have also been given [*Sonnerup,* 1979; *Baum and Bratenahl,* 1980*a*]. For a time-dependent reconnection process it seems more appropriate to describe the energy flow directly, as is done in this paper, rather than by an indirect rate coefficient.

Among the numerous observations of this experiment the following results appear to be the most important ones: (1) formation of a long flat neutral sheet stable against tearing for many Alfvén times; (2) buildup of hot dense plasma regions near the edges of the neutral sheet; (3) slow evolution of the classical fluid flow across the separatrix; (4) anomalous scattering of ions in the early phase of the reconnection process; (5) an internal space charge electric field along the neutral line, nearly canceling the applied inductive electric field; (6) large electrostatic fields and nonnegligible currents in the plane normal to the neutral line; (7) anomalous resistivity properly calculated from the generalized Ohm's law with all fields and currents measured; and (8) energy flow measurements showing an efficient transfer of electromagnetic energy into plasma heating rather than into fluid acceleration.

While many of the crucial questions in the reconnection problem seem to have been addressed, a few important problems still have to be investigated. These are the characteristics of plasma instabilities and their relation to the observed anomalous scattering of electrons and ions. Both

magnetic and electrostatic fluctuations have been detected in a wide frequency range and are presently under investigation. Furthermore, detailed measurements of the particle distribution functions would be desirable in order to determine instability mechanisms and the existence of runaway particles. Then it would be desirable to extend the time scale of the current rise and to operate in a regime where the ions are magnetized, both of which can be accomplished by reducing the ion mass. Presently, experiments in helium and hydrogen discharges are being performed.

Acknowledgments. The authors wish to thank T. McFadden for his expert help with the on-line data acquisition and M. Urrutia for his tireless technical assistance. The authors also appreciate the numerous discussions with F. Coroniti and C. Kennel. The research was supported by the Division of Atmospheric Sciences, National Science Foundation, under grant ATM79-21331 and by the Division of Atomic, Molecular, and Plasma Physics, National Science Foundation, under grant PHY79-23187.

The Editor thanks P. J. Baum for his assistance in evaluating this paper.

REFERENCES

Alexeff, I., G. E. Guest, J. R. McNally, Jr., R. V. Neidigh, and R. F. Scott, Doppler-broadened spectral emission from the turbulently heated plasma of burnout V, *Phys. Rev. Lett., 25,* 281–283, 1969.

Baum, P. J., A. Bratenahl, M. Kao, and R. S. White, Plasma instability at an X-type magnetic neutral point, *Phys. Fluids, 16,* 1501–1504, 1973.

Baum, P. J., and A. Bratenahl, Magnetic reconnection experiments, in *Advances in Electronics and Electron Physics,* vol. 54, edited by C. Marton, pp. 1–67, Academic, New York, 1980*a*.

Baum, P. J., and A. Bratenahl, Double layer formation during impulsive flux transfer events, *Rep. 80-01,* Inst. Geophys. Planet. Phys., Univ. of Calif., Los Alamos, N. Mex., 1980*b*.

Beeler, R., The IFTE in the DIPD, Ph.D. dissertation, Univ. Calif., Riverside, Univ. Microfilms, 1979.

Birn, J., Computer studies of the dynamic evolution of the geomagnetic tail, *J. Geophys. Res., 85,* 1214, 1980.

Bratenahl, A., and C. M. Yeates, Experimental study of magnetic flux transfer at the hyperbolic neutral point, *Phys. Fluids, 13,* 2696–2709, 1970.

Coroniti, F. V., F. L. Scarf, L. A. Frank, and R. P. Lepping, Microstructure of a magnetotail fireball, *Geophys. Res. Lett., 4,* 219–222, 1977.

Delcroix, J. L., *Plasma Physics,* p. 238, John Wiley, New York, 1965.

Dreicer, H., Electron and ion runaway in a fully ionized gas, *Phys. Rev., 115,* 238–249, 1959.

Frank, A. G., Experimental study of the conditions for the appearance of a neutral current sheet in a plasma: Some characteristics of the sheet, in *Neutral Current Sheets in Plasmas* (English Translation) *Proceedings of the P. N. Lebedev Physics Institute, Academy of Sciences USSR,* vol. 74, edited by N. G. Basov, p. 107, Consultants Bureau, New York, 1976.

Frank, L. A., K. L. Ackerson, and R. P. Lepping, On hot tenuous plasmas, fireballs, and boundary layers in the earth's magnetotail, *J. Geophys. Res., 81,* 5859–5881, 1976.

Frank, L. A., and K. L. Ackerson, Several recent findings concerning the dynamics of the earth's magnetotail, *Space Sci. Rev., 23,* 375–392, 1979.

Gekelman, W., and R. L. Stenzel, Magnetic field line reconnection experiments, 2, Plasma parameters, *J. Geophys. Res., 86,* 659–666, 1981.

Gekelman, W., R. L. Stenzel, and N. Wild, Magnetic field line reconnection experiments, 3, Ion acceleration, flows, and anomalous drag, *J. Geophys. Res.,* this issue, 1981.

Giovanelli, R. G., Chromospheric flares, *Mon. Not. R. Astron. Soc., 108,* 163–176, 1948.

Hamberger, S. M., and J. Jancarik, Experimental studies of electrostatic fluctuations in a turbulently heated plasma, *Phys. Fluids, 15,* 825–836, 1972.

Hayashi, T., and T. Sato, Magnetic reconnection: Acceleration, heating, and shock formation, *J. Geophys. Res., 83,* 217–220, 1978.

Langmuir, I., The interaction of electron and positive ion space charges in cathode sheaths, *Phys. Rev., 33,* 954, 1929.

Leboeuf, J. N., T. Tajima, and J. M. Dawson, Dynamic magnetic X-points, *Rep. PPG 542,* Univ. Calif. Plasma Phys. Group, Los Angeles, 1981.

McPherron, R. L., Magnetospheric substorms, *Rev. Geophys. Space Phys., 17,* 657–681, 1979.

Mirnov, S. V., and I. B. Semenov, Observation of disruptive-instability fine structure in a Tokamak, in *Plasma Physics and Controlled Nuclear Fusion Research (Proceedings of the 6th International Conference),* vol. 1, pp. 291–299, Int. At. Energy Agency, Vienna, 1977.

Niedner, M. B., and J. C. Brandt, Interplanetary gas, 23, Plasma tail disconnection events in comets: Evidence for magnetic field line reconnection at interplanetary sector boundaries?, *Astrophys. J., 223,* 655–670, 1978.

Ohyabu, N., and N. Kawashima, Neutral point discharge experiments, *J. Phys. Soc. Jpn., 33,* 496–501, 1972.

Ohyabu, N., S. Okamura, and N. Kawashima, Simulation experiment of the current dissipation and plasma acceleration in the neutral sheet, *J. Geophys. Res., 79,* 1977–1979, 1974*a*.

Ohyabu, N., S. Okamura, and N. Kawashima, Strong ion heating in a magnetic neutral point discharge, *Phys. Fluids, 17,* 2009–2013, 1974*b*.

Overskei, D., and P. Politzer, Plasma turbulence in the vicinity of a magnetic neutral line, *Phys. Fluids, 19,* 683, 1976.

Pellinen, R. J., and W. Heikkila, Energization of charged particles to high energies by an induced substorm electric field within the magnetotail, *J. Geophys. Res., 83,* 1544–1550, 1978.

Sato, T., T. Hayashi, T. Tamao, and A. Hasegawa, Confinement and jetting of plasmas by magnetic reconnection, *Phys. Rev. Lett., 41,* 1548–1551, 1978.

Sonnerup, B. U. Ö., Magnetic field line reconnection, in *Space Plasma Physics: The Study of Solar- System Plasmas,* vol. 2, part II, pp. 879–972, National Academy of Sciences, Washington D.C., 1979.

Spitzer, L., *Physics of Fully Ionized Gases,* p. 136, John Wiley, New York, 1962.

Stenzel, R. L., and W. Gekelman, Experiments on magnetic field line reconnection, *Phys. Rev. Lett., 42,* 1055–1057, 1979.

Stenzel, R. L., and W. Gekelman, Magnetic field line reconnection experiments, 1, Field topologies, *J. Geophys. Res., 86,* 649–658, 1981.

Syrovatskii, S. I., A. G. Frank, and A. Z. Khodzhaev, Current distribution near the null line of a magnetic field and turbulent plasma resistance, *Sov. Phys. Tech. Phys. (Engl. Transl.), 18,* 580–586, 1973.

Ugai, M., and T. Tsuda, Magnetic field-line reconnexion by localized enhancement of resistivity, Part 1, Evolution in a compressible MHD fluid, *J. Plasma Phys., 17,* 337–356, 1977.

Vasyliunas, V. M., Theoretical models of magnetic field line merging, 1, *Rev. Geophys. Space Phys., 13,* 303–336, 1975.

Zukakishvili, G. G., I. F. Kvartskhava, and L. M. Zukakishvili, Plasma behavior near the neutral line between parallel currents, *Sov. J. Plasma Phys., 4,* 405–410, 1978.

(Received February 11, 1981;
revised September 3, 1981;
accepted September 4, 1981.)